Elastic Effects on Phase Segregation in Alloys with External Stresses

C. A. Laberge,[1,*] P. Fratzl,[2] and J. L. Lebowitz[1]
[1]*Department of Physics and Mathematics, Rutgers University, Piscataway, New Jersey 08855-0849*
[2]*Institut für Festkörperphysik, Universität Wien, Boltzmanngasse 5, A-1090 Wien, Austria*
(Received 22 August 1995)

We investigate, via computer simulations, coherent phase segregation in a microscopic model alloy consisting of A and B atoms of unequal sizes on a square lattice. The effective Hamiltonian, obtained by minimization over the displacement of the atoms from their lattice positions, contains long range linear elastic interactions that cause the precipitates to be highly anisotropic. Under external load they acquire "wavy" long sides and align parallel to one of the axes. Their size, measured by the reciprocal of the number of A-B bonds, grows approximatively as $t^{1/3}$.

PACS numbers: 64.60.Qb, 05.70.Fh, 64.75.+g, 81.30.Mh

Directional coarsening or "rafting" is a well-known phenomenon observed when certain alloys containing misfitting precipitates, like nickel-based superalloys, are subjected to uniaxial external load. Depending on the material, a morphology consisting of either platelike structures perpendicular to or rodlike structures parallel to the stress direction develops [1–3]. Up to now modeling of the process has been done only macroscopically [2,4–6].

Here we investigate a conceptually simple microscopic model of this phenomenon in two dimensions. An extension to three dimensions, which is in principle straightforward, is being planned. The model of misfitting precipitates in an elastically anisotropic matrix generalizes one developed in [7], from here on referred to as I. It describes a system of A and B atoms with different sizes, on a planar square lattice $\mathcal{L}$ with periodic boundary conditions. The configuration is specified by $\mathbf{\Gamma}$, and the atomic positions by $\mathbf{U}$, with $\gamma(\mathbf{p}) = \pm 1$ and $\mathbf{u}(\mathbf{p})$ the deviation in the position from the lattice site $\mathbf{p} \in \mathcal{L}$. The atoms are connected by elastic springs that feel the difference of the atomic sizes, with longitudinal (L_+) and transverse (T_+) stiffness between nearest neighbors and springs with longitudinal stiffness ($L_\times$) between next nearest neighbors. There is also a nearest neighbor attraction J between like atoms.

In the present work we add to the Hamiltonian, given in Eq. (6) of I, an external stress corresponding to a homogeneous strain tensor $\boldsymbol{\epsilon}^0$. To model the linear dependence of the elastic constants on the transformation strain we introduce here a linear dependence of the coupling constants on the discrete strain $\eta(\mathbf{p})$ defined as in I by $\eta(\mathbf{p}) = \frac{1}{2}(R_A - R_B)[\gamma(\mathbf{p}) - (1 - 2\bar{c})]$, where R_A and R_B are the radii of A and B atoms (or ions), respectively, and $\bar{c}$ is the average concentration of A atoms in the alloy so that $\sum \eta(\mathbf{p}) = 0$. We let $L_+ \to L_+(1 + \alpha[\eta(\mathbf{p}) + \eta(\mathbf{p}')])$ and $L_\times \to L_\times(1 + \alpha[\eta(\mathbf{p}) + \eta(\mathbf{p}')]/\sqrt{2})$, where $\mathbf{p}$ and $\mathbf{p}'$ are lattice sites connected by the springs, and then keep in the energy only these terms in α that are of the form $\alpha\boldsymbol{\epsilon}^0$. This corresponds to considering a very weak dependence of the coupling constants on composition ($\alpha \ll 1$) and large external stresses. This gives the Hamiltonian

$$H(\mathbf{\Gamma}, \mathbf{V}; \boldsymbol{\epsilon}^0) = H_0(\mathbf{\Gamma}) + \tfrac{1}{2}\mathbf{V} \cdot \mathcal{A}(\mathbf{\Gamma}) \cdot \mathbf{V} + \mathbf{B}(\mathbf{\Gamma}) \cdot \mathbf{V}, \tag{1}$$

where H_0 is just the Ising Hamiltonian and $\mathbf{V}$ describes the displacement $\mathbf{U}$ relative to the homogeneous strain. We now minimize H with respect to $\mathbf{V}$. This corresponds physically to assuming that the displacement variables accommodate themselves very fast to the instantaneous composition $\mathbf{\Gamma}$. The minimization also corresponds to replacing the displacements by their average values for a specified configuration $\mathbf{\Gamma}$. We then obtain an effective Hamiltonian, which can be written conveniently in the form

$$H_e(\mathbf{\Gamma}; \boldsymbol{\epsilon}^0) = \frac{1}{2}\sum_{\mathbf{k}} \tilde{\Psi}(\mathbf{k})\,|\tilde{\gamma}(\mathbf{k})|^2, \tag{2}$$

where $\tilde{\gamma}(\mathbf{k})$, $\tilde{\Psi}(\mathbf{k})$ are the Fourier transforms of $\gamma(\mathbf{p})$ and the effective pair potential, $\Psi(\mathbf{p} - \mathbf{p}')$. $\tilde{\Psi}(\mathbf{k})$ is shown in Fig. 1. The potential $\Psi(\mathbf{r})$, which is a simple modification of that given by Eq. (12) in I to include the external strain, can be written as a sum of a "short" range part and a long range part $Y(\mathbf{r})$ whose continuum limit is the Fourier transform of $\hat{Y}(\hat{\mathbf{k}})$, $\hat{\mathbf{k}} = \mathbf{k}/|\mathbf{k}|$, given by $\lim_{|\mathbf{k}|\to 0} \tilde{\Psi}(\mathbf{k})$,

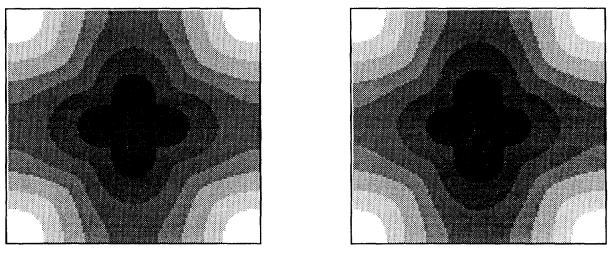

FIG. 1. Potential $\tilde{\Psi}(\mathbf{k})$ represented in the first Brillouin zone of the square lattice using a pseudogrey scale. The lowest values of the potential are dark, while the highest are white. The origin $\mathbf{k}$ is in the center of the picture. The left picture shows the case $b = d = 0$ (no external stress) and the right $b = 0, d = -0.4$ (uniaxial stress along the lines of the lattice).

 0031-9007/95/75(24)/4448(4)$06.00

less its circular average,

$$\hat{Y}(\hat{\mathbf{k}}) = Y_0[1 + a(\hat{k}_x\hat{k}_y)^2 + b(\hat{k}_x\hat{k}_y) + d(\hat{k}_x^2 - \hat{k}_y^2)]/[1 + g(\hat{k}_x\hat{k}_y)^2], \quad (3)$$

with $\hat{k}_x = \cos\theta$, $\hat{k}_y = \sin\theta$. The normalization $\int_0^{2\pi} \hat{Y}(\hat{\mathbf{k}})\, d\theta = 0$ gives $a = g - (4 + g)(2 + \sqrt{4 + g})/2$. The remaining constants Y_0, b, d, and g in (3) are related to the elastic properties of the material with b and d proportional to ϵ_{12}^0 and $\epsilon_{11}^0 - \epsilon_{22}^0$ corresponding to the external shear and uniaxial load (or stretch), respectively, and where g is a function of the cubic elastic constants c_{ij}, $g = (c_{11} - c_{12} - 2c_{44})(c_{11} + c_{12})/(c_{11}c_{44})$.

The important elastic effects on the coarsening all come from the long range elastic potential that decays like r^{-2} (r^{-3} in three dimensions). When $Y_0 = 0$ in (3), as happens when $R_A = R_B$, we expect the model to be in the same universality class as model B of [8]. In general, we expect that the kinetics will be described on the macroscopic scale by a Cahn-Hilliard type equation [9], for the local concentration

$$\frac{\partial c(\mathbf{r}, t)}{\partial t} = \nabla \cdot \left\{ \sigma(c) \nabla \frac{\delta}{\delta c(\mathbf{r}, t)} \int d\mathbf{r} \left[f(c) + \frac{1}{2} \lambda |\nabla c|^2 + \int d\mathbf{r}'\, Y(\mathbf{r} - \mathbf{r}') c(\mathbf{r}', t) c(\mathbf{r}, t) \right] \right\}. \quad (4)$$

Here $\sigma(c)$ is the mobility tensor that can be concentration dependent, and the integral over the system volume is the total free energy F of the nonuniform system driving the kinetics. The integrand consists of three terms: a "constrained" local free energy density $f(c)$ of the system with effective "short range" interactions, having a double well shape below the critical temperature with minima at the compositions of the two equilibrium phases, a gradient square term giving the contributions of the interfacial energy and the integral over $d\mathbf{r}'$, which can be rewritten as $\sum \hat{Y}(\hat{\mathbf{k}})\tilde{c}(\mathbf{k})$, representing the long range elastic energy contribution to F [10]. Equation (4), with a constant mobility σ, is essentially the one used by all continuum models [5,9–12] of spinodal decomposition with elastic effects. Some continuum models also consider an additional ordering field [11,12], and in some cases set the denominator in (3) equal to 1 [5] thereby replacing (4) by a differential equation in c and an auxiliary function $w = \nabla^{-2}c$. The morphologies obtained from these models are, at least visually, very similar to those obtained directly from the microscopic dynamics that we shall now describe.

Computer simulations were performed using the full interaction potential $\Psi(\mathbf{r})$, on a periodic 128×128 lattice at a temperature $kT/J = 1.8$, $T = 0.8T_c$, with T_c the Onsager critical temperature on a rigid square lattice, with and without external stress. Two "alloys" with concentration of (large) A atoms $\bar{c} = 0.5$ and $\bar{c} = 0.2$ were considered. The simulations were performed using Kawasaki dynamics with the Metropolis algorithm, where an exchange between a nearest neighbor pair chosen at random is performed if it leads to a decrease in total energy (2), otherwise it is only done with the probability $\exp(-\delta E/kT)$, $\delta E > 0$. Since the interaction potential is long range, a special truncation (to a range of ~20–30 lattice spaces), and updating procedure (described in I) was used. From the configurations, the structure function $|\tilde{\gamma}(\mathbf{k})|^2$ as well as the strain fields were deduced. These strain fields are $\epsilon_{11}(\mathbf{p}) = u_{1,1}$, $\epsilon_{22}(\mathbf{p}) = u_{2,2}$, and $\epsilon_{12}(\mathbf{p}) = u_{1,2} + u_{2,1}$, where $u_{i,j}$ is the lattice derivative of u_i in the direction j averaged over the four sites $(\mathbf{p}, \mathbf{p} + a\mathbf{e}_x, \mathbf{p} + a\mathbf{e}_y, \mathbf{p} + a\mathbf{e}_x + a\mathbf{e}_y)$ of a square "plaquette."

Figures 2 and 3 show snapshots of evolving configurations and the corresponding strain fields. The parameters in the long range elastic potential $\hat{Y}(\hat{\mathbf{k}})$ are $Y_0 = -0.57J$, $a = -5.0$, and $g = -2.4$ for the evolution without the external strain shown horizontally in Fig. 2. In terms of the macroscopic elastic constants they give an elastic anisotropy $(c_{11} - c_{12} - 2c_{44})/c_{44} = -1.4$, which describes a material like nickel or copper. Clearly, the elastic energy (without applied stress) has a tendency to favor the formation of stripes along the elastically soft direc-

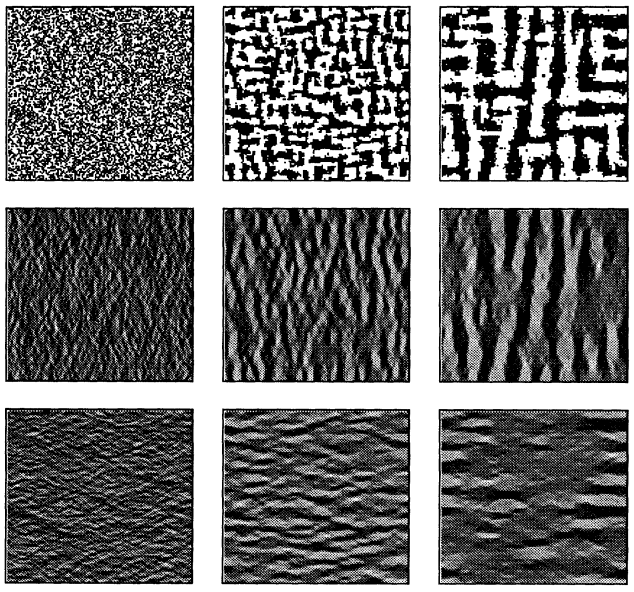

FIG. 2. Typical configurations (top row) obtained by letting the system evolve without any external stress. Times shown are $t = 0$ (random configuration), $t = 10^3$ MCS, and $t = 10^4$ MCS. The large A atoms are in black and the smaller B atoms in white and are in equal number. The second row shows the local strain ϵ_{11} for each configuration, while the third row shows ϵ_{22}. Dark (clear) regions with $\epsilon_{ii} > 0$ (<0) correspond to an expansion (compression) along the given i axis ($i = x, y$), average grey means $\epsilon_{ii} = 0$.

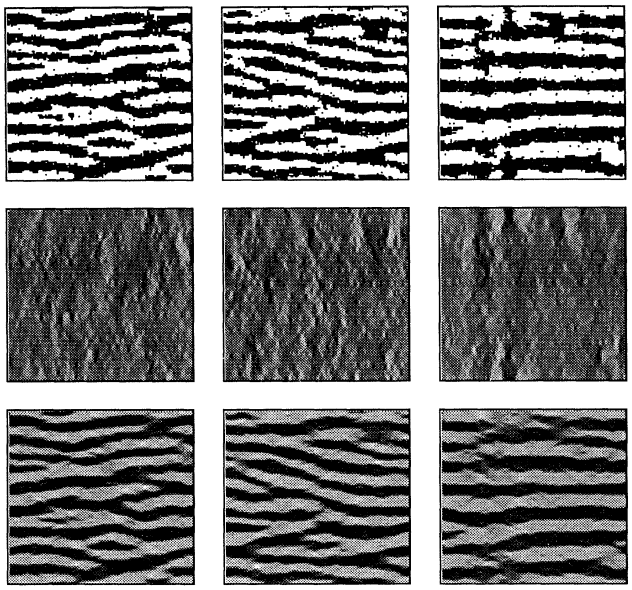

FIG. 3. Results obtained after 10^4 MCS with external stress ($\zeta = 0.1$) starting from the configurations shown in Fig. 2 prepared for 0, $t = 10^3$ MCS, and $t = 10^4$ MCS without external stress ($\zeta = 0$). The strains relative to the external (homogeneous) strain $\epsilon_{11} - \epsilon_{11}^0$ and $\epsilon_{22} - \epsilon_{22}^0$ of each configuration are shown in the second and third rows, respectively, with the same grey scale as in Fig. 1.

tions that are either horizontal or vertical in agreement with many earlier studies on the subject [5,11,13]. In the case of externally applied uniaxial stress (Fig. 3) where we took $b = 0$ and $d = -0.4$ in Eq. (3), the symmetry is broken and the stripes appear only with one orientation depending on the sign of b, in this case the horizontal. This is again in good agreement with theoretical [2,4,5] as well as experimental [1,14] studies of precipitate "rafting." The parallel stripes are extremely "wavy," and they thicken by a process where two stripes first touch and then join, reducing the number of stripes in the system. In the case where rafting starts from a random mixture of A and B atoms, this process dominates from the beginning. When rafting is started with a configuration prepared without external stress, the process starts with the breakdown of stripes with the "wrong" orientation. These are rearranged into horizontal stripes, and then thicken by the process mentioned earlier.

Looking now at the strain inside the lattice (second and third rows in Figs. 2 and 3), an interesting effect becomes immediately obvious: While for the case with external stress the picture of $\epsilon_{11} - \epsilon_{11}^0$ is almost uniformly grey (second row in Fig. 3) the one for $\epsilon_{22} - \epsilon_{22}^0$ reproduces exactly the stripe pattern seen in the configurations. This indicates that the horizontal strain inside the horizontal stripes is uniform, consistent with the periodic boundary conditions. In the direction perpendicular to the stripes, however, the lattice spacing is larger (smaller) where the atoms are larger (smaller). In this way, the small spacing in the black stripes compensates for the large spacing in the white stripes. A similar effect can be seen even in the case without external stress, where only the vertical stripes show up in the graph of ϵ_{11}, while only the horizontal ones can be seen in the graph of ϵ_{22}. From this it follows that the total elastic energy will not depend much on the thickness of the stripes. Indeed, a change in stripe thickness means only a redistribution of the strains (with roughly the same absolute value) in space. Since the elastic energy depends only on the sum of the squares of the strain, it will not change much (this holds for large enough stripes for which the dependence of the elastic potential on the length $|\mathbf{k}|$ of the vector $\mathbf{k}$ does not matter). This has been verified by calculating the evolution of elastic energy and the short-range energy separately as a function of time. Hence, the only driving force for the thickening of the stripes is the reduction of the total interface, just as in the case without elastic interactions. It is, therefore, quite reasonable that a suitably defined characteristic length should increase as $t^{1/3}$, t being the time, just as in the case without elastic interactions.

The number of A-B bonds in the horizontal and vertical directions, S_x and S_y, measure approximately the "surface area" perpendicular to these directions. In a typical coarsening process [15] with constant volume fraction of the phases one would expect the interface S to behave as $1/R$, where R is an average domain size. In analogy, we define the length scale R_s and an "aspect ratio" ρ by

$$R_s = 2L^2/(S_x + S_y), \qquad \rho = S_y/S_x . \tag{5}$$

R_s and ρ are plotted for a number of cases in Fig. 4 at $c = 0.5$. As can be seen in Fig. 4(a), R_s grows at essentially the same rate whether an external stress is applied to the system or not, except for the very final stages where finite size effects may become important. Such a $t^{1/3}$ growth is consistent with some experiments on nickel-based superalloys [14,16], but smaller growth exponents were found in a continuum model when external stress was applied [5]. However, in that case the thickness D of the stripes was obtained only over a rather narrow time range (typically a factor of 10). The data shown in [5] would, in fact, still be compatible with a time behavior in the form $D \approx D_0 + \lambda t^{1/3}$, D_0 and λ being constants. To decide whether the microscopic model presented here and the continuum model give the same or a different growth law for the domain, one would have to obtain data over a larger range of times for the continuum model.

The "aspect ratio" [see Fig. 4(b)], on the other hand, is strongly dependent on the external stress. As long as no stress is applied, ρ stays close to 1, since horizontal and vertical directions are equivalent in terms of the interaction potential. When an external stress is applied, this symmetry is broken and ρ increases. Surprisingly ρ never exceeds the value 2.5 even though rather long stripes are present in the system. The reason must be the

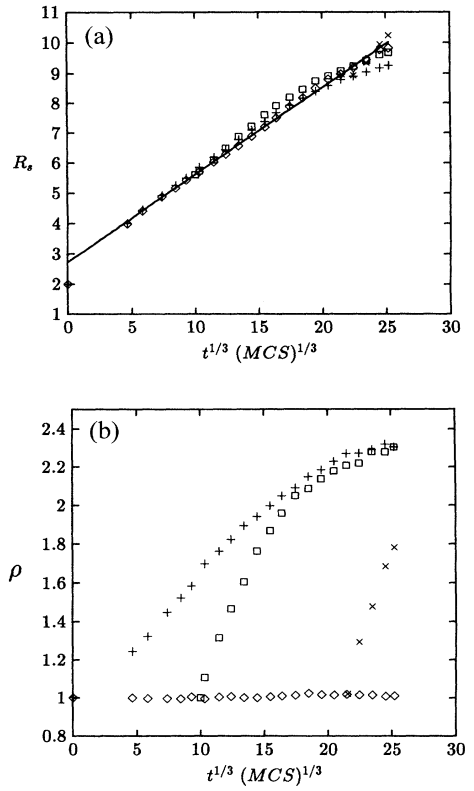

FIG. 4. Growth of (a) the typical length scale R_s and (b) the aspect ratio ρ defined in (5) plotted against (time)$^{1/3}$ for systems evolving with and without an external stress. These include runs starting from a homogeneous distribution with ($\diamond$) and without ($+$) external stress, as well as runs with external stress started after 10^3 ($\square$) and after 10^4 MCS ($\times$) pretreatment at the same temperature but without external stress. The full line in (a) is a linear fit to the data without external stress. All the points were obtained by averaging over 20 independent runs.

"waviness" of the stripes, which implies a large number of horizontal A-B bonds even when the stripes are horizontal. Nonetheless it is not quite clear why ρ seems to approach the same value in all cases after long enough times. We have also studied a number of runs starting with 8 or 16 perfectly straight stripes, where $\rho = \infty$. In all cases ρ started immediately to decrease as the stripes became wavy. After typically 5000 MCS, ρ reached a value close to 2.5 and did not change significantly anymore. Even though we have no explanation for this effect, it seems to indicate that the waviness is an intrinsic property of the model and corresponds to an instability of the straight lines with respect to deformations of the surface. In a more general context, it may be related to the general instability of flat surfaces in stressed solids [17], see also [18]. Most interestingly, the stripes observed in experiments [1,14], as well as in the continuum model studied by Nishimori and Onuki [5] are also quite wavy.

This work was supported by NSF Grant No. 92-134244-20946. We thank M. Fährmann, V. Gorentsveig, A. Khachaturyan, R. Kohn, O. Paris, O. Penrose, and Y. Wang for discussions. P. F. also acknowledges support by the Fonds zur Förderung der Wissenschaftlichen Forschung (Project S5601).

*Present address: Department of Physics, Virginia Polytechnic Institute, Blacksburg, VA 24061–0435.

[1] J. K. Tien and S. M. Copley, Metall. Trans. **2**, 215 (1971).
[2] J. C. Chang and S. M. Allen, J. Mater. Res. **6**, 1843 (1991).
[3] For a recent short review see, e.g., S. Socrate and D. M. Parks, Acta Metall. Mater. **41**, 2185 (1993).
[4] W. C. Johnson, M. B. Birkenpas, and D. E. Laughlin, Acta Metall. **36**, 3149 (1988).
[5] H. Nishimori and A. Onuki, Phys. Rev. B **42**, 980 (1990).
[6] J. Gayda and D. J. Srolovitz, Acta Metall. **37**, 641 (1989).
[7] P. Fratzl and O. Penrose, Acta Metall. Mater. **43**, 2921 (1995).
[8] P. C. Hohenberg and B. I. Halperin, Rev. Mod. Phys. **49**, 435 (1977).
[9] J. S. Langer, in *Solids Far from Equilibrium,* edited by C. Godreche (Cambridge University Press, Cambridge, England, 1992).
[10] J. Cahn, Acta Metall. **10**, 179 (1962).
[11] Y. Wang, L.-Q. Chen, and A. G. Khachaturyan, Acta Metall. Mater. **41**, 279 (1993).
[12] C. Sagui, A. M. Somoza, and R. Desai, Phys. Rev. E **50**, 4865 (1994).
[13] P. Fratzl and O. Penrose, Acta Metall. Mater. (to be published).
[14] T. Miyazaki, K. Nakamura, and H. Mori, J. Mater. Sci. **14**, 1827 (1979).
[15] P. Fratzl, J. L. Lebowitz, O. Penrose, and J. Amar, Phys. Rev. B **44**, 4794 (1991).
[16] M. Fährmann, P. Fratzl, O. Paris, E. Fährmann, and W. C. Johnson, Acta Metall. Mater. **43**, 1007 (1995).
[17] D. J. Srolovitz, Acta Metall. Mater. **37**, 621 (1989).
[18] O. L. Alerhand *et al.,* Phys. Rev. Lett. **61**, 1973 (1988); J. Tersoff and E. Pehlke, Phys. Rev. Lett. **68**, 816 (1992); J. Tersoff and F. K. LeGoues, Phys. Rev. Lett. **72**, 3570 (1994); Y. H. Xie *et al.,* Phys. Rev. Lett. **73**, 3006 (1994).

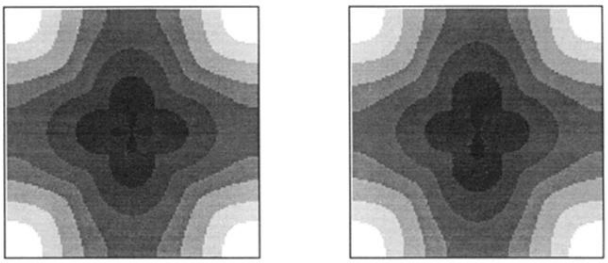

FIG. 1. Potential $\tilde{\Psi}(\mathbf{k})$ represented in the first Brillouin zone of the square lattice using a pseudogrey scale. The lowest values of the potential are dark, while the highest are white. The origin $\mathbf{k}$ is in the center of the picture. The left picture shows the case $b = d = 0$ (no external stress) and the right $b = 0, d = -0.4$ (uniaxial stress along the lines of the lattice).

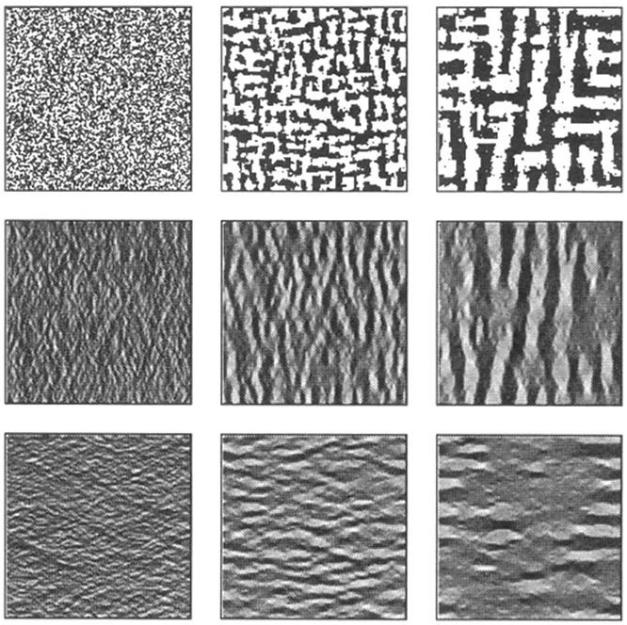

FIG. 2. Typical configurations (top row) obtained by letting the system evolve without any external stress. Times shown are $t = 0$ (random configuration), $t = 10^3$ MCS, and $t = 10^4$ MCS. The large A atoms are in black and the smaller B atoms in white and are in equal number. The second row shows the local strain ϵ_{11} for each configuration, while the third row shows ϵ_{22}. Dark (clear) regions with $\epsilon_{ii} > 0$ (<0) correspond to an expansion (compression) along the given i axis ($i = x, y$), average grey means $\epsilon_{ii} = 0$.

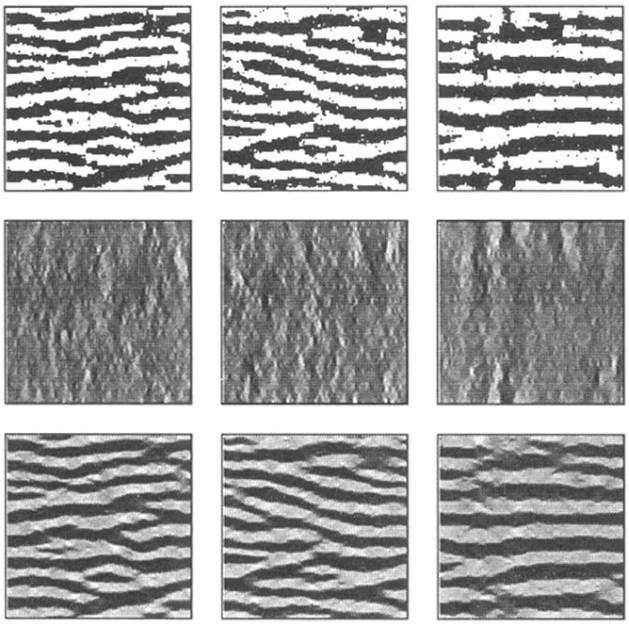

FIG. 3. Results obtained after 10^4 MCS with external stress ($\zeta = 0.1$) starting from the configurations shown in Fig. 2 prepared for 0, $t = 10^3$ MCS, and $t = 10^4$ MCS without external stress ($\zeta = 0$). The strains relative to the external (homogeneous) strain $\epsilon_{11} - \epsilon_{11}^0$ and $\epsilon_{22} - \epsilon_{22}^0$ of each configuration are shown in the second and third rows, respectively, with the same grey scale as in Fig. 1.